# Influence of Subgrid Variability on Surface Hydrology

S. J. GHAN, J. C. LILJEGREN, W. J. SHAW, J. H. HUBBE, AND J. C. DORAN

*Pacific Northwest National Laboratory, Richland, Washington*

(Manuscript received 12 December 1996, in final form 31 March 1997)

ABSTRACT

A 6.25-km resolution dataset of meteorology, vegetation type, and soil type for a domain covering a typical global climate model grid cell is used to drive a land surface physics model for a period of 6 months. Additional simulations are performed driving the land surface physics model by spatially averaged meteorology, spatially averaged vegetation characteristics, spatially averaged soil properties, and spatially averaged meteorology, vegetation characteristics, and soil properties. By comparing the simulated water balance for the whole domain for each simulation, the relative influence of subgrid variability in meteorology, vegetation, and soil are assessed. Subgrid variability in summertime precipitation is found to have the largest effect on the surface hydrology, with a nearly twofold increase on surface runoff and a 15% increase in evapotranspiration. Subgrid variations in vegetation and soil properties also increase surface runoff and reduce evapotranspiration, so that surface runoff is 2.75 times as great with subgrid variability than without and evapotranspiration is 19% higher with subgrid variability than without.

## 1. Introduction

Soil hydrology is highly nonlinear. As surface soil becomes saturated with water, excess water runs off in streams. If the parameters that influence surface soil moisture vary widely within a global climate model (GCM) grid cell, the grid cell mean runoff, soil moisture, and evapotranspiration could be very sensitive to the treatment of subgrid variability.

The parameters that control surface hydrology include meteorology (primarily precipitation, but also wind speed, temperature, and humidity), downward radiation (solar and longwave), soil characteristics (porosity, hydraulic conductivity, thermal conductivity, and albedo), and vegetation characteristics (leaf area index, fractional vegetation cover, stomatal resistance, and root depth). Of these, precipitation is the most likely candidate for driving subgrid variations in surface hydrology, particularly in the summertime when precipitation is primarily convective and hence can be highly heterogeneous. One might expect to find much more runoff and hence less soil moisture and evapotranspiration if subgrid variations in precipitation are accounted for.

However, because soil moisture is an integrator of temporal variability on timescales of up to a month, it is not necessarily the instantaneous distribution of the precipitation that is important for surface hydrology. Because precipitation systems typically propagate, the monthly mean precipitation is likely to be much more homogeneous than the instantaneous precipitation. Thus, it is not at all obvious that even highly convective summertime precipitation can produce enough subgrid variability in surface hydrology that such variability must be treated when estimating the grid cell mean runoff, soil moisture, and evapotranspiration.

These issues are not new. Using simplified distributions of rainfall and surface characteristics, Milly and Eagleson (1988) found the potential for a serious underestimation of surface runoff if the areal variability of precipitation associated with storms of various scales and types is ignored. Entekhabi and Eagleson (1989) used analytic distributions of rainfall and soil moisture conditions to examine the sensitivity of runoff, bare soil evaporation efficiency, and transpiration efficiency to soil type and climatic forcing. Pitman et al. (1990) used a surface hydrology model driven by meteorology simulated by a GCM to investigate the influence of the subgrid distribution of precipitation on the surface water balance, but assumed an idealized function for the subgrid distribution of precipitation. Dolman and Gregory (1992) tested the behavior of two parameterizations of rainfall interception and found that the interception losses were sensitive to the fractional area of the GCM grid cell that was covered by rain. Avissar (1992) described a statistical–dynamical approach to representing land surface heterogeneity in atmospheric models and found large differences in fluxes computed with this approach compared with those obtained from a big leaf model. Bonan et al. (1993) considered the influence of subgrid variations in leaf area index, stomatal resistance,

*Corresponding author address:* Dr. Steven J. Ghan, Pacific Northwest National Laboratories, P.O. Box 999, Richland, WA 99352.
E-mail: sj_ghan@pnl.gov

© 1997 American Meteorological Society

Unauthenticated | Downloaded 10/18/21 11:53 PM UTC

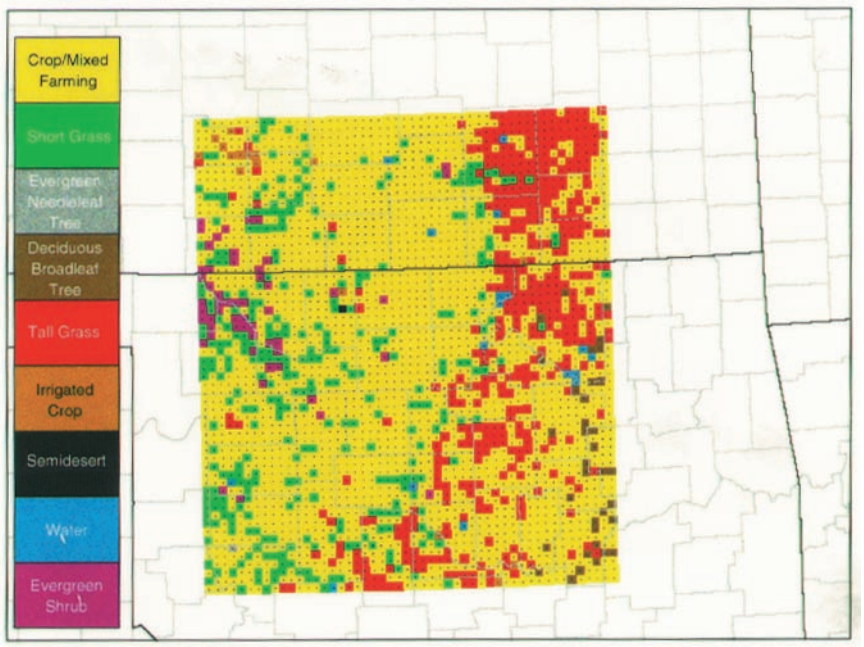


FIG. 1. Distribution of soil types for the experiment domain.

and soil moisture on the surface energy balance, but used a spatially uniform precipitation prescribed periodically. Famiglietti and Wood (1995) examined the effects of spatial variability and scale on areally averaged evapotranspiration; they found that for scales greater than a few kilometers, statistical distribution functions of the dominant process controls, such as soil type, gave more realistic results than the use of spatially averaged parameters and that the effect was to increase the modeled evapotranspiration. Noilhan and Lacarrere (1995) addressed the influence of subgrid variations in roughness length, surface resistance, vegetation cover, leaf area index, albedo, saturation moisture content, and saturated hydraulic conductivity on the surface water and energy balance, but did not address the influence of subgrid variations in precipitation. Seth et al. (1994) divided a GCM cell into 36 subgrid cells to study the effects of subgrid-scale vegetation and climate specification on surface fluxes and hydrology; they showed that energy partitioning at the surface, surface stress, and runoff could all be significantly affected. Mölders and Raabe (1996) considered realistic variations in all of these fields but simulated only a single day and hence could not address the issue of soil moisture storage.

In this paper we present a preliminary evaluation of the relative importance of subgrid variations in each of the parameters that control surface hydrology. The emphasis is on the use of observations to drive a physically based model of the land surface water and energy balance. The results, while dependent upon the particular land surface model employed, are representative of what the sensitivity would be using other models.

## 2. Approach

To characterize the subgrid variability in surface hydrology, we drive a land surface model (the Biosphere–Atmosphere Transfer Scheme—BATS: Dickinson et al. 1993) with meteorology, radiation, soil characteristics, and vegetation characteristics estimated at 6.25-km resolution from observations within a domain characteristic of a GCM grid cell (300 km on a side). The domain is the U.S. Department of Energy Atmospheric Radiation Measurement and Clouds and Radiation Testbed (CART) in Kansas and Oklahoma (Fig. 1), where meterology, radiation, soil, and vegetation characteristics are measured at as fine a resolution as anywhere in the world. Although this region is not noted for its surface heterogeneity, we shall find significant effects of surface heterogeneity on surface hydrology. Other regions can be expected to exhibit larger effects.

The meterological data used as input for the BATS scheme were gathered from several measurement networks in Oklahoma and Kansas. These included the Oklahoma Mesonetwork [also called the Oklahoma Mesonet; Brock et al. (1995)], the Kansas State University mesonetwork, National Weather Service hourly reports, the CART Surface Meteorological Observing System (SMOS) stations, and the WSR-88D NEXRAD precipitation data from Arkansas Red Basin River Forecast

Unauthenticated | Downloaded 10/18/21 11:53 PM UTC

TABLE 1. Meteorological data sources.

| Source | Stations | Interval | Variable | | | | | |
|---|---|---|---|---|---|---|---|---|
| | | | Pressure | Temperature | Humidity | Solar | Wind | Precip. |
| Oklahoma mesonet | 111 | 5 min | X | X | X | X | X | |
| National Weather Service | 40 | 1 h | X | X | X | | X | |
| Kansas mesonet | 4 | 1 h | X | X | X | X | X | |
| SMOS | 5 | 0.5 h | X | X | X | | X | |
| NEXRAD | 335 × 159 | 1 h | | | | | | X |

Center radars (for precipitation only). In general, there were numerous stations both inside and beyond the edges of the interpolation grid. Table 1 summarizes variables obtained from each network and their reporting intervals.

To produce interpolated fields, data (except precipitation) were first checked for invalidity and then averaged or interpolated as appropriate to form time series of half-hour values for each variable at each reporting station. The data for each half hour were then checked for outliers and interpolated to a grid centered on the CART Central Facility using a method employing multiquadric basis functions described by Nuss and Titley (1994). The grid extended 362.5 km in the north–south direction and 312.5 km east–west. Grid spacing was 6.25 km.

On occasion, entire measurement networks failed to report for a number of hours. While the interpolation scheme performed very well when constrained by data, it was poor at extrapolation. To keep values at least reasonable over the entire domain, eight ''anchor points'' were defined beyond the corners and edge midpoints of the domain. Coordinates were chosen so that these anchor points would be located 1.5 times the distance from the nearest edge point to the center of the domain. The anchor points were assigned values based on a $1/r^2$ weighted average of the nearest three valid data, no matter how far away they occurred. The anchor points were then treated in the interpolation scheme as an independent dataset.

We created precipitation fields differently from those for the other variables because of the high density (4-km spacing) of the radar measurements. To have applied the interpolation method described above would have required the inversion of unmanageably large matrices. Instead, we performed a simple average weighted by 1/r to all precipitation measurements within 5 km of each grid point.

The soil characteristics are described according to the BATS representation of 12 different soil types ranging from sand to loam to clay. For each soil type, BATS assigns values of soil porosity, hydraulic conductivity, thermal conductivity, albedo, and other parameters. The soil types were assigned from the State Soil Geographic Data Base (Soil Conservation Service 1993), which has a spatial resolution of 1 km. Figure 1 shows the distribution of soil types for the domain. Of the 2900 grid points in the domain, 922 were found to be silt loam, 844 sandy loam, 328 loam, 319 silty clay loam, 168 loamy sand, 149 clay loam, and 132 sand.

The vegetation characteristics are determined from the BATS representation of 18 different vegetation types. The vegetation type at each station was determined from the U.S. Geological Survey land cover characteristics dataset CD-ROM, which uses the Advanced Very High Resolution Radiometer (AVHRR) and Normalized Difference Vegetation Index (NDVI) to assign 28 vegetation classes at 1-km resolution. These 28 vegetation classes were folded into the 18 BATS vegetation classes. The class at each 6.25-km grid point was determined from the class at the 1-km pixel closest to the center of the grid point. Figure 2 shows the distribution of vegetation types. Of the 2900 grid points in the domain, 2007 were found to be crops–mixed farming, 443 tall grass, 325 short grass, 54 evergreen shrub, 35 deciduous broadleaf tree, 17 irrigated crop, and 17 inland water. For each vegetation class, the BATS scheme assigns values for fractional vegetation cover, minimum stomatal resistance, surface depth, albedo, and other parameters.

The BATS scheme also estimates leaf area index (LAI) from the vegetation type and surface temperature. Because this fails to account for the effects of harvesting, we have replaced the BATS estimate of LAI with an estimate of LAI from the NDVI measured by the AVHRR satellite. NDVI values covering the period from 9 February 1995 to 13 August 1995 were used. Satellite images were sought for days with clear or mostly clear skies over the CART; 22 images were eventually selected to produce time series of NDVI values at each grid point. The resultant data were typically fairly noisy and often showed significant deviations from a slowly varying time series. To correct for this, we used a modification of the robust least squares method described by Sellers et al. (1996). In the Sellers et al. approach, monthly mean NDVI values were fit to a Fourier series to produce a first estimate of the annual cycle of NDVI values for $1° \times 1°$ grid elements. For our data we used Legendre polynomials instead of sines and cosines for the fitting functions. These gave improved fits to our data, which did not extend over a full year and thus did not exhibit a primary annual cycle of variation. Using our fitting procedure, we generated values for NDVI at 5-day intervals and linearly interpolated those values to obtain values at 1-day intervals. The LAI was estimated

Unauthenticated | Downloaded 10/18/21 11:53 PM UTC

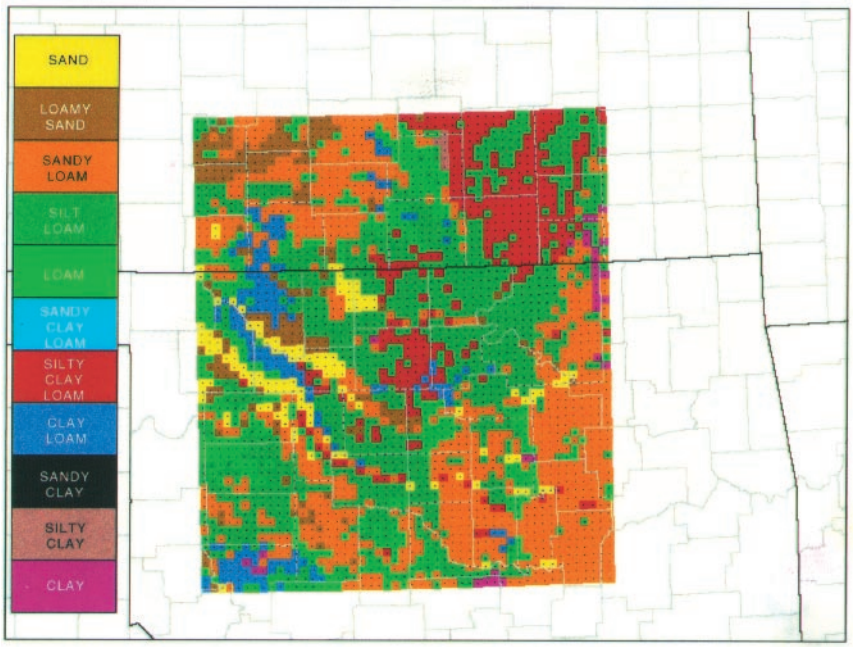


FIG. 2. Distribution of vegetation types for the experiment domain.

from NDVI following Sellers et al. (1996), as described in the appendix.

Downward longwave radiation is estimated from the measured surface air temperature, humidity, and downward solar radiation using Brunt's equation (Monteith 1973).

The selected analysis period is June–August 1995. Summertime conditions were chosen because precipitation is most likely to be convective, and hence heterogeneous, during this time.

The simulations at each point were initialized on 1 March 1995, which provides 3 months for soil moisture to ''spin up'' before the analysis period. The surface soil and foilage temperatures are initialized with the observed surface air temperature. The deep soil temperature is initially set at 8°C. Soil moisture for all layers and all points is initialized at the field capacity, defined such that gravitational drainage is 2 mm $day^{-1}$ for every soil type. The minimum and maximm stomatal resistance are prescribed as 100 and 20 000 s $m^{-1}$, respectively, for all vegetation types. The displacement height of vegetation is prescribed as 1 m for all vegetation types.

To assess the importance of accounting for spatial variability in various parameters, we drove BATS at each grid point, first accounting for the full spatial variability of all parameters, and then with various parameters averaged over the domain. By averaging a different parameter in separate simulations, we can isolate the influence of the spatial variability in each parameter on the spatial mean response. Parameters considered are precipitation, vegetation characteristics, soil characteristics, radiation, and wind speed.

For soil and vegetation properties, averaging was performed following Noilhan and Lacarrere (1995), weighting with respect to frequency of each soil and vegetation type. Note that for some parameters, such as minimum surface resistance and surface roughness, inverse or logarithmic means are more appropriate than arithmetic means. We have also performed experiments in which we simply adopted the parameters associated with the dominant soil and vegetation types for the domain (silt loam and crops–mixed farming), but the results did not agree as well with the heterogeneous case as does the averaging method of Noilhan and Lacarrere. For properties that cannot be averaged, such as the presence or absence of irrigation, the dominant property was chosen.

## 3. Results

To understand the results, consider the water balance for leaf surfaces and for the root zone, as treated by BATS. These balances can be expressed

$$\frac{\partial \mathrm{RW}}{\partial t} = P_g + D + I + F - E_g - E_v - R + K - G,$$

$$\frac{\partial \mathrm{LW}}{\partial t} = P - P_g - D - E_l.$$

Here RW and LW are the water in the root zone and on the leaves, respectively; $P$ and $P_g$ are total precipi-

Unauthenticated | Downloaded 10/18/21 11:53 PM UTC

TABLE 2. Spatial—temporal mean simulated surface hydrology.

| Simulation | Process (mm day$^{-1}$) | | | | | | | | | | |
|---|---|---|---|---|---|---|---|---|---|---|---|
| | $P_g$ | $D$ | $I$ | $F$ | $E_g$ | $Ev$ | $E_l$ | $E$ | $R$ | $K$ | $G$ |
| HET | 0.15 | 4.15 | 0.08 | 0.04 | 0.80 | 3.26 | 0.33 | 4.39 | 0.77 | 0.45 | 0.53 |
| HOMOP | 0.18 | 3.27 | 0.07 | 0.04 | 0.83 | 3.02 | 1.18 | 5.03 | 0.40 | 0.42 | 0.31 |
| HOMOV | 0.15 | 4.14 | 0.00 | 0.00 | 0.70 | 3.54 | 0.34 | 4.57 | 0.70 | 0.32 | 0.29 |
| HOMOS | 0.16 | 4.14 | 0.04 | 0.04 | 0.92 | 3.21 | 0.33 | 4.46 | 0.70 | 0.68 | 0.68 |
| HOMOR | 0.15 | 4.14 | 0.08 | 0.04 | 0.80 | 3.26 | 0.34 | 4.39 | 0.76 | 0.45 | 0.52 |
| HOMOW | 0.15 | 4.15 | 0.07 | 0.04 | 0.79 | 3.27 | 0.32 | 4.38 | 0.77 | 0.44 | 0.52 |
| LIN | 0.19 | 3.24 | −0.06 | 0.00 | 0.84 | 3.26 | 1.19 | 5.27 | 0.25 | 0.51 | 0.20 |
| HOMO | 0.19 | 3.20 | 0.00 | 0.00 | 0.84 | 3.31 | 1.24 | 5.39 | 0.28 | 0.40 | 0.13 |

tation and precipitation reaching the ground (i.e., not intercepted by leaves), respectively; $D$ is water dripping from leaves to the ground; $I$ is irrigation of the soil; $F$ is inflow (for lakes and marshes); $E_g$, $E_v$, and $E_l$ are evapotranspiration from the ground, from leaf stomata, and from leaf water, respectively; $R$ is surface runoff; $K$ is diffusion from below the root zone; and $G$ is gravitational drainage from the root zone.

The water balance for the root zone and vegetation together can be expressed

$$\frac{\partial(\mathrm{RW} + \mathrm{LW})}{\partial t} = P + I + F - E - R + K - G,$$

where $E = E_g + E_v + E_l$ is the total evapotranspiration.

Table 2 lists the spatial–temporal mean of these components of the surface-water balance for all simulations. The simulations are denoted HET (fully heterogeneous), HOMOP (all parameters heterogeneous except precipitation), HOMOV (all parameters heterogeneous except vegetation), HOMOS (all parameters heterogeneous except soil), HOMOR (all parameters heterogeneous except radiation), HOMOW (all parameters heterogeneous except wind), and HOMO (all parameters homogeneous). A linear combination (LIN) is described later.

Before considering the sensitivity experiments, let us first examine the water balance for the fully heterogeneous case (HET). Almost all of the precipitation is intercepted by vegetation, with only 0.15 mm day$^{-1}$ directly striking the ground out of 4.63 mm day$^{-1}$ total precipitation. Most of the intercepted precipitation drips to the ground, with only 0.33 mm day$^{-1}$ evaporating from the leaf water. Of the water reaching the ground, most of it (3.26 mm day$^{-1}$) transpires through vegetation, with only 0.80 mm day$^{-1}$ evaporating from the ground itself and only 0.77 mm day$^{-1}$ running off the surface. The small amount that drains below the root zone is nearly balanced by diffusion from below the root zone. Irrigation and inflow are nearly negligible for this region. Total evaporation $E$ is dominated by transpiration $E_v$.

Now consider the simulation with homogeneous precipitation (HOMOP). The precipitation striking the ground is nearly the same as in the heterogeneous case. However, because the precipitation is spread evenly over all points, leaf drip is reduced by 0.88 mm day$^{-1}$. This reduction in the supply of water to the ground reduces runoff from 0.77 to 0.40 mm day$^{-1}$, a 48% reduction, and reduces gravitational drainage from 0.53 to 0.31 mm day$^{-1}$. Because runoff and gravitational drainage are nonlinear functions of soil moisture, these reductions in runoff and drainage occur even though the mean root zone soil moisture hardly changes at all.

Transpiration $E_v$ is reduced from 3.26 mm day$^{-1}$ for heterogeneous precipitation to 3.02 mm day$^{-1}$ for homogeneous precipitation. This occurs because $E_v = 0$ for wet vegetation, which is much more common for homogeneous precipitation. Evaporation of leaf water ($E_l$) increases substantially, from 0.33 to 1.18 mm day$^{-1}$, as the precipitation is spread over more leaves. Evaporation from the ground increases slightly, from 0.80 to 0.83 mm day$^{-1}$, as the surface layer moistens in response to the reduced runoff. The total evaporation increases from 4.39 to 5.03 mm day$^{-1}$, largely because of the increased evaporation of leaf water.

When vegetation is assumed to be homogeneous (HOMOV), the leaf water balance is surprisingly similar to the heterogeneous case. The precipitation intercepted by plants ($P - P_g$), leaf drip $D$, and evaporation from leaves $E_l$ are all virtually identical to the heterogeneous simulation. This suggests that there is a low spatial correlation between precipitation and vegetation properties in the fully heterogeneous case. However, the root zone water balance is somewhat different, largely because irrigation is absent since irrigated land is not the dominant surface type. Points that were irrigated crops in the fully heterogeneous case are not irrigated and hence are drier for HOMOV, so that the spatial mean gravitational drainage is reduced from 0.53 to 0.29 mm day$^{-1}$, runoff is reduced from 0.77 to 0.70 mm day$^{-1}$, and evaporation from the surface is reduced, from 0.80 to 0.70 mm day$^{-1}$. Transpiration increases, from 3.26 to 3.54 mm day$^{-1}$, apparently as a result of the averaging of vegetation properties. Because the changes in surface evaporation and transpiration partially cancel, the total evaporation only increases from 4.39 to 4.57 mm day$^{-1}$.

When soil is assumed to be homogeneous (HOMOS), evaporation from the ground increases from 0.80 to 0.92 mm day$^{-1}$, not because of changes in soil moisture (which are very small), but because of changes in soil properties, that is, maximum hydraulic conductivity $K_0$

Unauthenticated | Downloaded 10/18/21 11:53 PM UTC

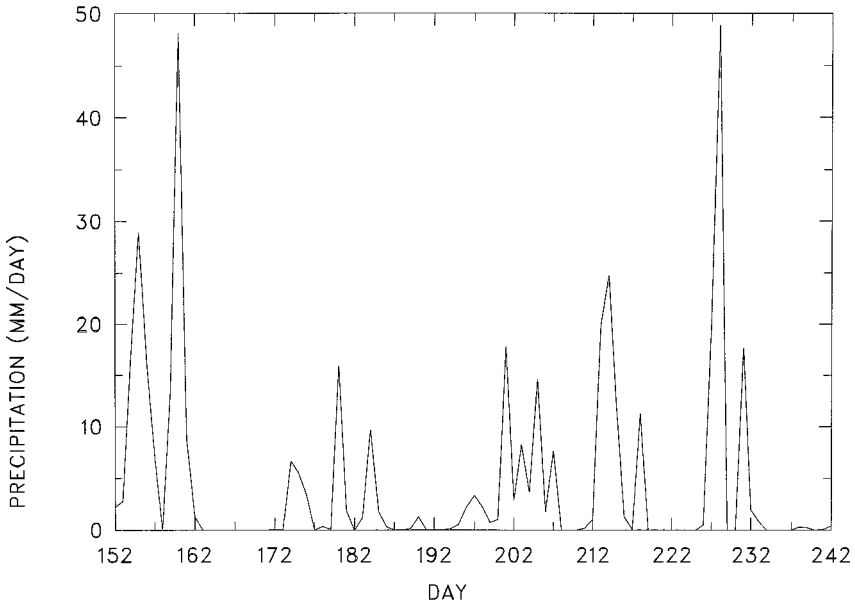


FIG. 3. Daily and area mean precipitation used to drive BATS for June–August 1995.

and the Clapp and Hornberger (1978) parameter *B*, both of which influence the maximum moisture flux that the soil can sustain. Because the dependence of the maximum sustainable moisture flux on $K_0$ and $B$ is highly nonlinear, averaging $K_0$ and $B$ does not yield the same average moisture flux as when $K_0$ and $B$ are not averaged. Similarly, transpiration decreases from 3.26 to 3.21 mm day$^{-1}$ through the nonlinear dependence of root resistance on *B*. Surface runoff decreases from 0.77 to 0.70 mm day$^{-1}$ and gravitational drainage increases from 0.53 to 0.68 mm day$^{-1}$ because poorly conducting points, where water runs off rather than drains in the heterogeneous case, drain water better in the HOMOS case; again, the nonlinear dependence of transport on soil properties is responsible for the difference between the HOMOS and HET cases.

The simulations with homogeneous radiation and winds yield results very similar to the fully heterogeneous case.

When all parameters are spatially averaged (HOMO), the results are suprisingly close to the linear combination of the results for spatially averaging each set of parameters. In Table 2, the row LIN lists the linear superposition of results from spatially averaging each set of parameters:

$$\text{LIN} = \text{HET} + \sum_{i=1}^{I} (\text{HOMO}i - \text{HET}),$$

where $i = P, V, S, R, W$. The HOMO and LIN values agree to within 0.1 mm day$^{-1}$ for all fields. The differences between HOMO and LIN are smaller than differences between HET and other simulations for all fields except irrigation, which, because it is determined such that the soil remains saturated, depends fundamentally on whether the vegetation is irrigated crop and is very sensitive to the saturated hydraulic conductivity of the soil. For the other fields, by comparing the difference between HOMO*i* and HET with the difference between HOMO and HET, we can compare the effect of averaging each parameter to the effect of averaging all parameters. We find that mean leaf drip *D*, evaporation of leaf water $E_l$, and runoff *R* are most strongly affected by averaging precipitation, that irrigation and inflow are most affected by averaging vegetation, that evaporation from the ground $E_g$ and diffusion to the root zone *K* are most affected by averaging vegetation and soil properties, that transpiration $E_v$ is most affected by averaging precipitation and vegetation properties, and that drainage *G* is influenced by averaging precipitation, vegetation, and soil properties.

To see how systematic the averaging biases can be, Figs. 3–8 show time series of the daily–domain mean precipitation, leaf drip, evaporation of leaf water, transpiration, surface runoff, and drainage for the simulations with full heterogeneity, average precipitation, average soil properties, and average vegetation properties. The domain mean precipitation (Fig. 3), which is of course the same in each experiment, exhibits variability on timescales of days, with peak daily accumulations of up to 50 mm. Leaf drip (Fig. 4) follows precipitation very closely, with leaf drip for the simulation with homogeneous precipitation somewhat less than for the simulations with heterogeneous precipitation. Evaporation of leaf water (Fig. 5) is clearly much higher with homogeneous precipitation than with heterogeneous precipitation. Transpiration (Fig. 6) is consequently much less with homogeneous precipitation than with heterogeneous precipitation because leaf water is pres-

Unauthenticated | Downloaded 10/18/21 11:53 PM UTC

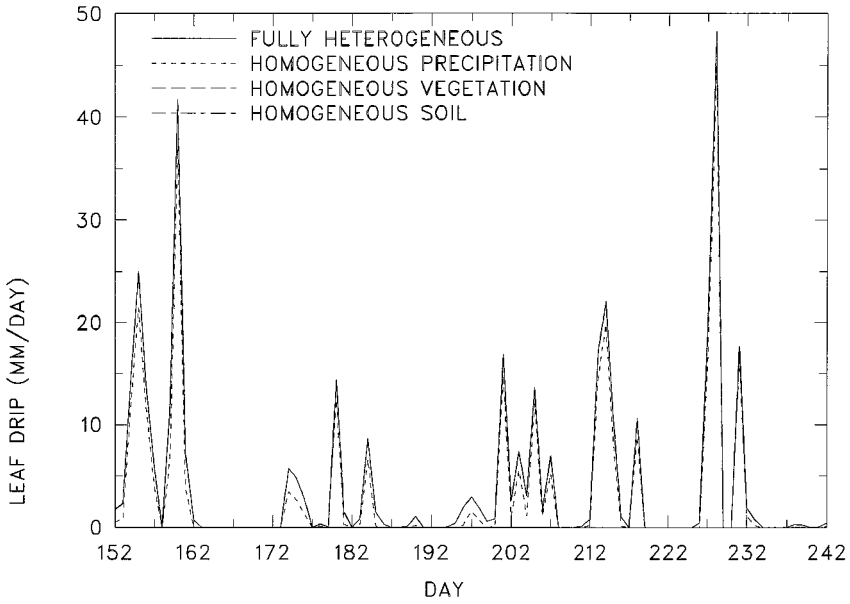


FIG. 4. Daily and area mean leaf drip simulated by BATS with full variability in forcing and surface properties, with spatially averaged precipitation, with spatially averaged vegetation properties, and with spatially averaged soil properties.

ent at more grid cells. Runoff (Fig. 7) follows precipitation but is reduced for homogeneous precipitation because leaf drip is lower. Drainage from the root zone (Fig. 8) varies more slowly than runoff because it does not depend upon the instantaneous precipitation; it is systematically higher with homogeneous soil than with heterogeneous soil and is significantly lower with homogeneous vegetation and precipitation.

## 4. Conclusions

In our application of the BATS model with observed summertime data, we have found that neglecting spatial variations in precipitation reduces the simulated summertime runoff by 48% and enhances summertime evaporation by 15%. Neglecting subgrid variations in vegetation properties reduces the simulated summertime

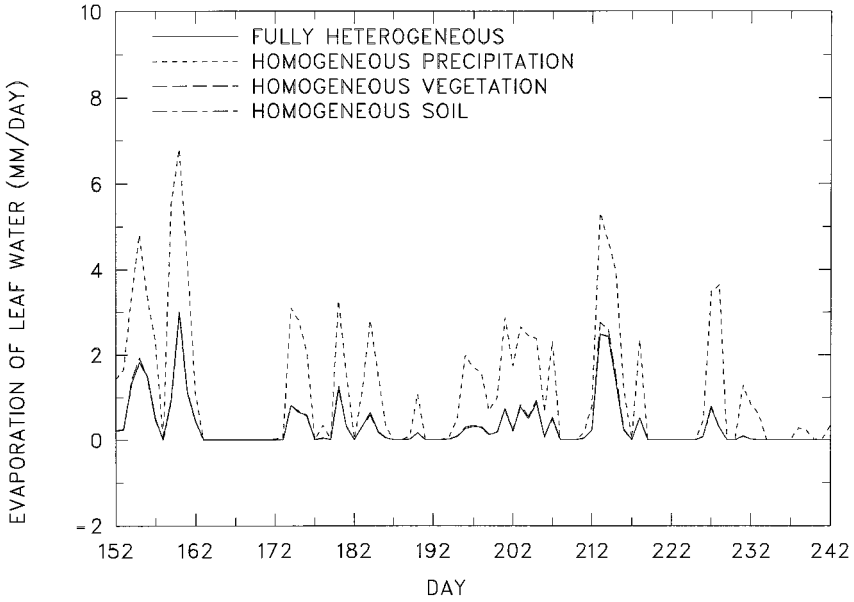


FIG. 5. As in Fig. 4 but for evaporation of leaf water.

Unauthenticated | Downloaded 10/18/21 11:53 PM UTC

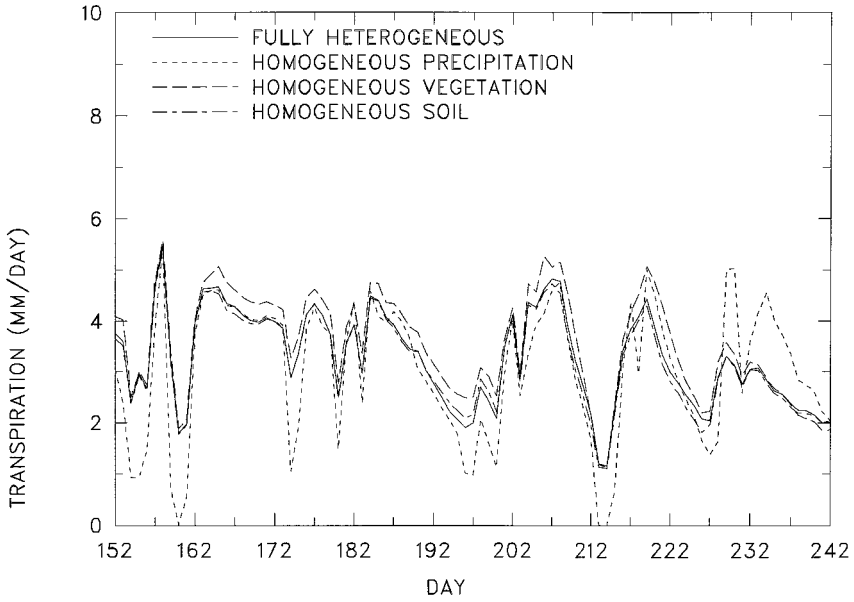


FIG. 6. As in Fig. 4 but for evapotranspiration.

runoff by 9% and enhances summertime evaporation by about 4%. Neglecting subgrid variations in soil properties reduces the simulated summertime runoff by 9% and enhances summertime evaporation by only 2%. Neglecting subgrid variations in soil and vegetation properties as well as meteorological forcing reduces the simulated summertime runoff by 64% and enhances summertime evaporation by 23%. Whether these biases are considered significant depends upon the application of interest. These conclusions depend of course upon the BATS model used to estimate the sensitivity of the surface hydrology to external parameters. Other models may yield somewhat different results.

This paper has only considered spatial variations on scales from 6.25 km to roughly 300 km. Spatial variations on larger scales would be explicitly resolved by a GCM, but spatial variations on scales smaller than 6.25 km may also be important. Although vegetation type, leaf area index (both of which are derived from AVHRR satellite measurements), and soil texture are available at 1-km resolution, precipitation measurements are available at the relatively coarse spatial res-

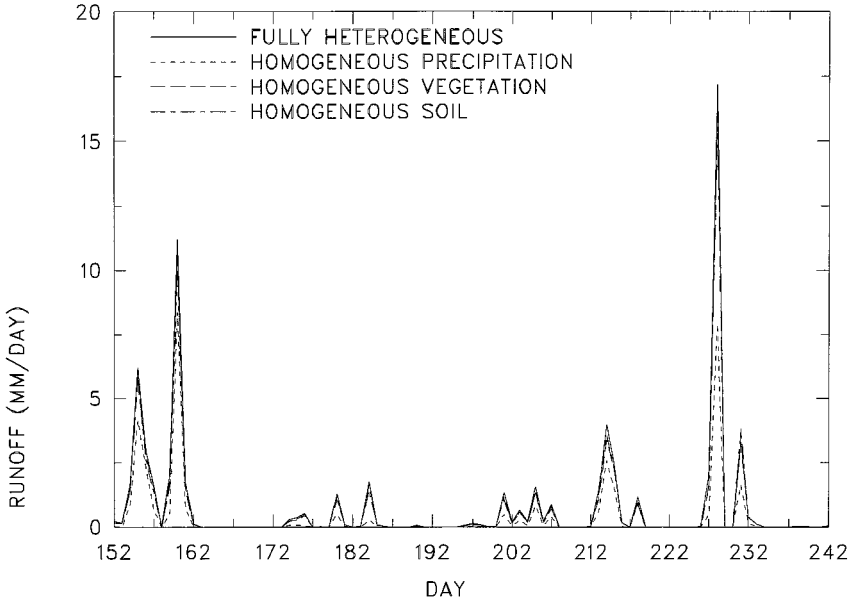


FIG. 7. As in Fig. 4 but for surface runoff.

Unauthenticated | Downloaded 10/18/21 11:53 PM UTC

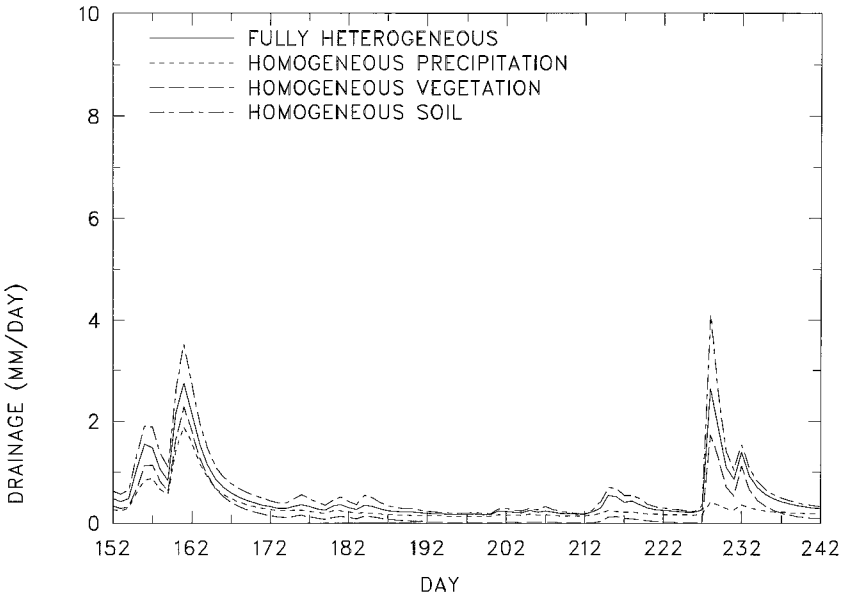


FIG. 8. As in Fig. 4 but for gravitational drainage.

olution of 4 km. Thus, until precipitation measurements are available at finer resolution, the influence of variability on scales much finer than 6.25 km cannot be evaluated.

In other seasons we would expect the influence of subgrid variations in precipitation to be less than during the summer, but in other regions the influence of subgrid variations in surface properties could be much greater than in the southern Great Plains.

*Acknowledgments.* This research was supported by the Environmental Sciences Division of the U.S. Department of Energy (DOE) as part of the Atmospheric Radiation Measurement Program, which is part of the DOE Biological and Environmental Research Program. Pacific Northwest National Laboratory is operated for the DOE by Battelle Memorial Institute under Contract DE-AC06-76RLO 1830.

## APPENDIX A

### Estimation of Leaf Area Index

The calculation of LAI from the NDVI derived from AVHRR imagery closely follows the methodology described by Sellers et al. (1996). First the simple ratio (SR), which is the ratio of the reflectance in the near-infrared (AVHRR channel 2) to that in the visible (channel 1), is computed from the NDVI:

$$\mathrm{SR} = \frac{1 + \mathrm{NDVI}}{1 - \mathrm{NDVI}}.$$

The fraction of photosyntheically active radiation (FPAR) absorbed by the vegetation canopy is then computed according to

$$\mathrm{FPAR} = \frac{\mathrm{SR} - \mathrm{SR}_{\mathrm{min},i}}{\mathrm{SR}_{\mathrm{max},i} - \mathrm{SR}_{\mathrm{min},i}}(\mathrm{FPAR}_{\mathrm{max},i} - \mathrm{FPAR}_{\mathrm{min},i}),$$

where the subscript $i$ refers to the land-use classification in the grid cell and the maximum and minimum values of SR and FPAR are tabulated by Sellers et al. (1996) for each of the biomes in the Simple Biosphere 2 ($SiB_2$) model. For use in BATS, the $SiB_2$ biomes were mapped according to Table A1.

Green leaf LAI, $L_g$, is determined from the FPAR according to

$$L_g = L_{g\mathrm{max},i}\frac{\mathrm{FPAR}}{\mathrm{FPAR}_{\mathrm{max},i}},$$

where $L_{g\mathrm{max},i}$ is the maximum green leaf LAI for the $i$th land-use class tabulated by Sellers et al. According to Sellers et al., this formulation, for which the green leaf LAI is directly proportional to the FPAR, is applicable to cases where the vegetation within the grid cell is clustered. We used this instead of another formulation provided by Sellers et al. that is applicable to homogeneous vegetation for which $L_g$ is proportional to the logarithm of FPAR. Our choice was motivated by simulations carried out using $SiB_2$ for a location where local measurements were available to drive the model. The simulations showed that over the entire growing season the clustered formulation produced superior agreement with the local flux measurements. The formulation for clustered vegetation appears to better represent the real world where cold-tolerant species (e.g., $C_3$ grasses), which dominate earlier in the year, are replaced by heat-tolerant species during the summer (e.g., $C_4$ grasses) as shown by Sellers et al. (1992), as well as situations where winter wheat (which is harvested in early June) is followed by a second crop.

Unauthenticated | Downloaded 10/18/21 11:53 PM UTC

TABLE A1. Mapping BATS and $SiB_2$ land-use types.

| BATS type | $SiB_2$ type |
|---|---|
| 1 Crop–mixed farming | 9 Agriculture or $C_3$ grassland |
| 2 Short grass | 9 Agriculture or $C_3$ grassland |
| 3 Evergreen needleleaf trees | 4 Evergreen needleleaf trees |
| 4 Deciduous needleleaf trees | 5 Deciduous needleleaf trees |
| 5 Deciduous broadleaf trees | 2 Deciduous broadleaf trees |
| 6 Evergreen broadleaf trees | 1 Evergreen broadleaf trees |
| 7 Tall grass | 6 $C_4$ grassland |
| 8 Desert | 7 Shrubs with bare soil |
| 9 Tundra | 8 Dwarf trees and shrubs |
| 10 Irrigated crop | 9 Agriculture or $C_3$ grassland |
| 11 Semidesert | 7 Shrubs with bare soil |
| 12 Ice | NA |
| 13 Bog or marsh | NA |
| 14 Inland water | NA |
| 15 Ocean | NA |
| 16 Evergreen shrub | 8 Dwarf trees and shrubs |
| 17 Deciduous shrub | 8 Dwarf trees and shrubs |
| 18 Mixed woodland | 3 Broadleaf and needleleaf trees |

The total LAI, $L_T$, is given by $L_T = L_g + L_{s,i} + L_d$, where $L_{s,i}$ is the stem area index for the given land-use class and $L_d$ is the dead leaf area index. The fraction of green leaves within the canopy, $G$, is then given by

$$G = \frac{L_g}{L_T}.$$

As long as the green leaf area is nondecreasing [e.g., $L_g(t + \Delta t) \geq L_g(t)$], then $L_d = 0$. However, once $L_g$ begins to decrease, $L_d$ is set equal to the difference between the largest value of $L_g$ attained and the current value of $L_g$. Sellers et al. (1996) remove dead leaves that are more than 30 days old from the canopy, reasoning that they are either eaten or fall off; we have implemented this criterion using a recursive low-pass filter:

$$L_g(t + \Delta t) = L_g(t + \Delta t) - L_{d,\text{old}}(t)$$

$$L_{d,\text{old}}(t + \Delta t) = aL_d(t + \Delta t) + (1 - a)L_{d,\text{old}}(t), \quad (8)$$

where $a = 0.002$ causes the value of $L_{d,\text{old}}$ to represent a moving, exponentially weighted average of the previous values of $L_d$ with a time constant of 500 $\Delta t$. For 30-min time steps this amounts to about 10.5 days. If $L_g$ begins to increase again, signaling growth (e.g., a second crop), then $L_d$ is reset to zero.

## REFERENCES


Avissar, R., 1992: Conceptual aspects of a statistical–dynamical approach to represent landscape subgrid-scale heterogeneities in atmospheric models. *J. Geophys. Res.,* **97,** 2729–2742.

Bonan, G., D. Pollard, and S. L. Thompson, 1993: Influence of subgrid-scale heterogeneity in leaf area index, stomatal resistance, and soil moisture on grid-scale land–atmosphere interactions. *J. Climate,* **6,** 1882–1897.

Brock, F. V., K. C. Crawford, R. L. Elliott, G. W. Cuperus, S. J. Stadler, H. L. Johnson, and M. D. Eilts, 1995: The Oklahoma Mesonet: A technical overview. *J. Atmos. Oceanic Technol.,* **12,** 5–19.

Clapp, R. B., and G. M. Hornberger, 1978: Emperical equations for hydraulic properties. *Water Resour. Res.,* **14,** 601–604.

Dickinson, R. E., A. Henderson-Sellers, and P. J. Kennedy, 1993: Biosphere–Atmosphere Transfer Scheme (BATS) version 1e as coupled to the NCAR Community Climate Model. NCAR Tech. Note NCAR/TN-387+STR, 72 pp. [NTIS PB64-106150.]

Dolman, A. J., and D. Gregory, 1992: The parametrization of rainfall interception in GCMs. *Quart. J. Roy. Meteor. Soc.,* **118,** 455–467.

Entekhabi, D., and P. S. Eagleson, 1989: Land surface hydrology parameterization for atmospheric general circulation models including subgrid scale spatial variability. *J. Climate,* **2,** 816–831.

Famiglietti, J. S., and E. F. Wood, 1995: Effects of spatial variability on areally averaged evapotranspiration. *Water Resour. Res.,* **31,** 699–712.

Milly, P. C. D., and P. S. Eagleson, 1988: Effect of storm scale on surface runoff volume. *Water Resour. Res.,* **24,** 620–624.

Mölders, N., and A. Raabe, 1996: Numerical investigations on the influence of subgrid-scale surface heterogeneity on evapotranspiration and cloud processes. *J. Appl. Meteor.,* **35,** 782–795.

Monteith, J. L., 1973: *Principles of Environmental Physics.* Edward Arnold, 242 pp.

Noilhan, J., and P. Lacarrere, 1995: GCM grid-scale evaporation from mesoscale modeling. *J. Climate,* **8,** 206–223.

Nuss, W. A., and D. W. Titley, 1994: Use of multiquadric interpolation for meteorological objective analysis. *Mon. Wea. Rev.,* **122,** 1611–1631.

Pitman, A. J., A. Henderson-Sellers, and Z.-L. Yang, 1990: Sensitivity of regional climates to localized precipitation in global models. *Nature,* **346,** 734–737.

Sellers, P. J., C. J. Tucker, G. J. Collatz, S. O. Los, C. O. Justice, D. A. Dazlich, and D. A. Randall, 1992: A global 1° by 1° NDVI data set for climate studies. Part 2: The generation of global fields of terrestrial biophysical parameters from the NDVI. *Int. J. Remote Sens.,* **15,** 3519–3534.

——, S. O. Los, C. J. Tucker, C. O. Justice, D. A. Dazlich, G. J. Collatz, and D. J. Randall, 1996: A revised land surface parameterization (SiB2) for atmospheric GCMs. Part II: The generation of global fields of terrestrial biophysical parameters from satellite data. *J. Climate,* **9,** 706–737.

Seth, A., F. Giorgi, and R. E. Dickinson, 1994: Simulating fluxes from heterogeneous land surfaces: Explicit subgrid method employing the Biosphere–Atmosphere Transfer Scheme (BATS). *J. Geophys. Res.,* **99,** 18 651–18 667.

Soil Conservation Service, 1993: The state soil geographic data base (STATSGO) data users guide. Misc. Publ. 1492, 88 pp. [Available from National Cartography and GIS Center, USDA, P.O. Box 6567, Fort Worth, TX 76115.]


Unauthenticated | Downloaded 10/18/21 11:53 PM UTC